ELSEVIER

Microelectronics Journal 33 (2002) 689–696

Microelectronics Journal

www.elsevier.com/locate/mejo

# Four different approaches for the measurement of IC surface temperature: application to thermal testing

Josep Altet[a], Stefan Dilhaire[b], Sebastian Volz[c], Jean-Michel Rampnoux[b], Antonio Rubio[a,*], Stephane Grauby[b], Luis David Patino Lopez[b], Wilfrid Claeys[b], Jean-Bernard Saulnier[c]

[a]*Department of Electronic Engineering, UPC, Campus Nord, Building C4, 08034 Barcelona, Spain*
[b]*Centre de Physique Moléculaire Optique et Hertzienne, CPMOH, University of Bordeaux I, 352 Cours de la libération, 33405 Talence Cedex, France*
[c]*Laboratoire d'Etudes Thermiques, Ecole Nationale Superieur de Mechanique et d'Aerotechnique, LET-ENSMA-BP, 109-86960 Futuroscope Cedex, France*

Accepted 21 May 2002

**Abstract**

Silicon die surface temperature can be used to monitor the health state of digital and analogue integrated circuits (IC). In the present paper, four different sensing techniques: scanning thermal microscope, laser reflectometer, laser interferometer and electronic built-in differential temperature sensors are used to measure the temperature at the surface of the same IC containing heat sources (hot spots) that behave as faulty digital gates. The goal of the paper is to describe the techniques as well as to present the performances of these sensing methods for the detection and localisation of hot spots in an IC. 

*Keywords:* Thermal testing; Scanning thermal microscopy; Laser reflectometry; Laser interferometry; Built-in temperature sensors; Thermal couplings; Integrated circuits

## 1. Introduction

Temperature is a physical magnitude that has been used as a parametric test observable for integrated circuits (ICs) in different scenarios: failure analysis [1,13], reliability prevention [15,16] and detection of structural defects in an IC. Such defects include structural problems in the microelectronic circuit [11,18] or in the package structure [3,5,7]. All these techniques are generically termed thermal testing techniques.

The feasibility of the different thermal testing procedures is inherently linked to the existence and performance of temperature monitoring techniques. The purpose of monitoring the temperature is to obtain an image of the thermal map of its surface. This thermal map can cover the entire surface or merely a region of it. It can be continuous (with a given lateral resolution) or discrete (temperature at finite and specific number of points of the surface: punctual measurements).

Thermal monitoring techniques can be categorised into three main groups: optical techniques, mechanical techniques and built-in temperature sensors. Optical methods are based on measurements of characteristics of light, either emitted or reflected by the surface of the circuit under test (CUT). Optical methods can be classified in methods that require a coating (liquid crystals [2,6,7], microscopic fluorescence [8,9]) and those which merely take measurements of the sample surface, with no contact requirements (infrared emission [6,12,14], thermoreflectometers, interferometers). Mechanical methods include techniques based on mechanical contact between the sensor and the surface to be measured. This category includes the atomic force microscopy, with different tips: thermocouples [10], Pt resistors. Finally, temperature can be measured with electronic sensors built-in with the CUT. These sensors are based on the temperature dependency of the electrical characteristics of semiconductor devices. The output signal of built-in temperature sensors can be proportional either to absolute temperature or to the difference in temperature at two points on the silicon surface. This leads to the categorisation of temperature sensors into two groups: absolute and differential. The electrical output signal of a sensor can be, respectively, written for the two categories as:

$$\text{Signal}_{\text{Out}} = S_{\text{A}}T + C$$

* Corresponding author.
*E-mail addresses:* antonio.rubio@upc.es (A. Rubio), pepaltet@eel.upc.es (J. Altet).

0026-2692/02/$ - see front matter 
PII: S0026-2692(02)00051-4

$$\text{Signal}_{\text{Out}} = S_{\text{D}}(T_2 - T_1)$$

where $S_{\text{A}}$ is the absolute sensitivity of the absolute temperature sensor, $S_{\text{D}}$ the differential sensitivity of the differential temperature sensor, $C$ an offset constant that may be zero and $T$, $T_2$ and $T_1$ are temperatures at different points on the silicon surface.

Absolute temperature sensors are used to monitor the working temperature of the CUT and eventually correct its operating point if it is working beyond its reliability limit [15,16]. In Refs. [15,16] forward biased PN junctions are used as temperature sensors for that purpose. Another application of absolute temperature sensors is the thermal testing of packages [3–5]. Examples of CMOS absolute temperature sensors for thermal testing applications can be found in Refs. [17,18].

Differential temperature sensors are used to detect alterations of the thermal map of the silicon due to changes in the power dissipated by its devices. They are insensitive to temperature increases that may offset the thermal map of the silicon surface, e.g. ambient temperature changes or leakage current increases in CMOS circuits.

The goal of this paper is to present measurements and to compare performances of four of the temperature monitoring techniques listed above: scanning thermal microscopy, laser reflectometry (LRT), laser interferometry (LIT) and electronic built-in differential temperature sensors. We will compare the different techniques in terms of cost, bandwidth (if dynamic measurements can be performed), complexity of the required equipment and applicability (the ability to take measurements at any point of the IC), hot spot location ability and capacity to carry out point measurements or full thermal maps.

An IC sample that has been specially designed to characterise thermal couplings has been used as a CUT. In this IC sample, several individually controllable heat sources (MOS transistors with sizes of (10 μm)/(1.2 μm) and connected in diode configuration) have been positioned along with BiCMOS differential temperature sensors. The technology features two layers of metal and the sample is coated with oxide and passivation layers. The power supply voltage ($V_{\text{dd}}$) can be increased up to 5 V.

We will evaluate each technique in terms of its ability to perform three different types of thermal measurements:

1. DC measurements, in which the heat source dissipates a DC power and the temperature is measured when the thermal steady state is reached. This technique is appropriate to perform on-line testing of the integrated system as a whole and to carry out failure analysis of quiescent hot spots.
2. AC measurements, in which the heat source dissipates a periodic power function $P(t) = P_{\text{DC}} + P_{\text{AC}} \sin(wt)$. The temperature at one point on the silicon surface can be described by $T(t) = T_{\text{DC}} + T_{\text{AC}} \sin(wt + \phi)$. Both $T_{\text{AC}}$ and $\phi$ can be measured using a lock-in amplifier. These measurements are used either to characterise thermal coupling impedance values in the frequency domain or to diagnose defective circuits.
3. Transient measurements: the waveform of the temperature at a given point on the surface is obtained when the heat source dissipates a power pulse of magnitude $P_{\text{MAX}}$ and duration $D$, with capabilities that are similar to those mentioned above.

The organisation of this paper is as follows. Sections 2–5 present the main characteristics of the scanning thermal microscope, laser reflectometer, laser interferometer and the differential built-in temperature (DBT) sensor, respectively, as well as the thermal measurements performed with each equipment. In Section 6, a discussion about the obtained results is presented and finally, Section 7 provides the conclusion.

## 2. Scanning thermal microscope

The scanning thermal microscope (SThM—®Topometrix) is a conventional atomic force microscope (AFM) mounted with a specific probe. The AFM system allows us to control the tip position and contact force with the sample. Monitoring is performed with a feedback loop between the signals of three $x$–$y$–$z$ piezo-electrical ceramics carrying the tip cantilever and four photodiodes tracking a laser beam which reflects on the probe. The probe is a Wollaston wire shaped as a tip and etched to uncover the core platinum wire (Fig. 1). The Pt wire is used as a thermal resistor: at constant input current, the tip voltage is measured while scanning the surface so that the Pt electrical resistance can be estimated at each point on the sample surface. The AFM is used in contacting mode therefore thermal equilibrium is achieved between the probe and the surface. A preliminary calibration allows us to relate temperature variations to electrical resistance variations to an accuracy within 10%. The contact radius of the tip can be estimated to 50 nm [19], its diameter being 5 μm. A laser beam reflects on the mirror to detect $z$-deflections of the cantilever with nanometric precision, allowing us to extract topographic maps of the IC surface.

Fig. 2 shows measurements performed with the SThM. (a) shows a processed topographic image while a

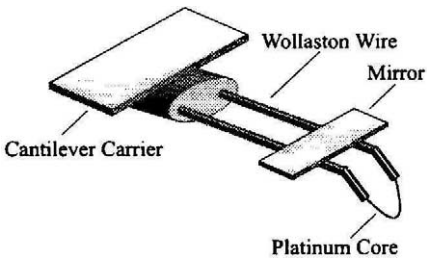


Fig. 1. Schematic of the thermal probe.

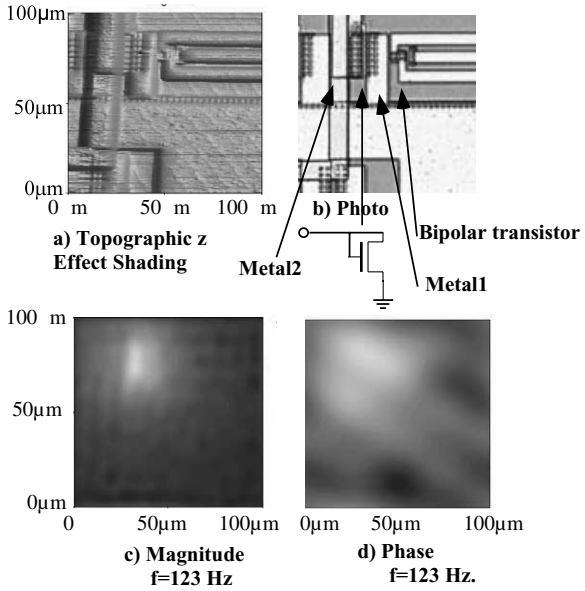


Fig. 2. Topographic and AC temperature measurements.

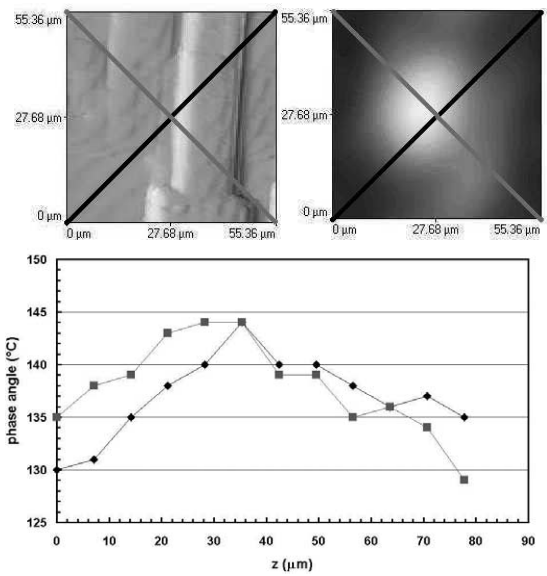


Fig. 3. Topographical and DC thermal amplitudes images of the hot spot location (up-left and right respectively). Black and grey lines represent axis along which the phase profile was acquired as reported in the bottom graph.

photograph of the same location of the layout is provided in (b). Comparing (a) and (b) allows us to easily identify and locate the metal lines and devices (i.e. the MOS transistors acting as heat sources and a bipolar transistor). (c) and (d) show AC (magnitude and phase, respectively) temperature measurements obtained when the heat source is modulated at a frequency of 123 Hz and the thermal signal is filtered at the same reference frequency. Although the oxide and passivation layers placed over the silicon attenuate the temperature signal, the system sensitivity is sufficient to detect and locate the hot spot. Similar results have been obtained in DC measurements. Higher sensitivity is observed in phase measurements than in amplitude AC or DC measurements. Note that the metal line, which acts as a heat spreader, attenuates both the phase and amplitude signals. The time needed to extract these images is about 2 min. The duration of the scanning per unit area depends on the resolution. For instance, if the image size is set to: $50 \times 50\ \mu m^2$ divided into 200 lines and one line being scanned in 1s, the scanning rate is $16\ s/\mu m^2$ and the total scanning time is of course of the order of 3 min.

The SThM set-up affords a high spatial resolution for heat source tracking. After scanning the zone under interest, the probe can be positioned to a set of points in order to improve the averaging and filtering of local measurements. As example, Fig. 3 reports the spatial dependence of the phase signal over the heat spot.

The non-symmetrical phase profiles confirm heat spreading by the metal line. At $z = 35\ \mu m$, equal phase values are obtained. This $z$-coordinate corresponds to the intersection point between both profiles. The fact that equal values are measured reveals the high accuracy of the method. The difference between both profiles in the range of lower $z$ values reflects a difference in the subsurface material composition.

This information is apparently not accessible through DC scanning and emphasises the good sensitivity of the method.

## 3. Laser reflectometer

Thermoreflectance exploits the proportionality between the variation of a material's reflection coefficient and the surface temperature changes of that material. If a laser beam is focused on a silicon surface and the reflected light is sensed with a photodiode, variations of the current, $I$, generated by changes of the reflection coefficient can be related to the variations of the temperature, $\Delta T$, of the area to which the laser points [20]:

$$\Delta T = \psi^{-1} \frac{\Delta I}{I}$$

The constant $\psi$ depends on the material and the light wavelength, and typical values can be found in the relevant literature. However, when the laser beam reaches the silicon surface through silicon dioxide and passivation layers, this coefficient is affected by a scaling factor that can be greater or smaller than unity, depending on the thickness of these layers [21]. Usually a calibration stage is needed to obtain the exact value of $\psi$. Results reported in Ref. [22] show the laser probe to be a fast surface thermometer (DC to 150 MHz) with an excellent lateral resolution (1 μm) and large dynamics ($\Delta T$ from $10^2$ to $10^{-3}$ K).

Fig. 4 shows the heat source used for the measurements.

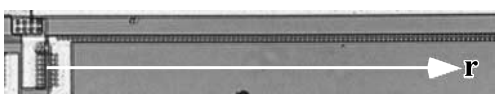


Fig. 4. Heat source used for the laser measurements.

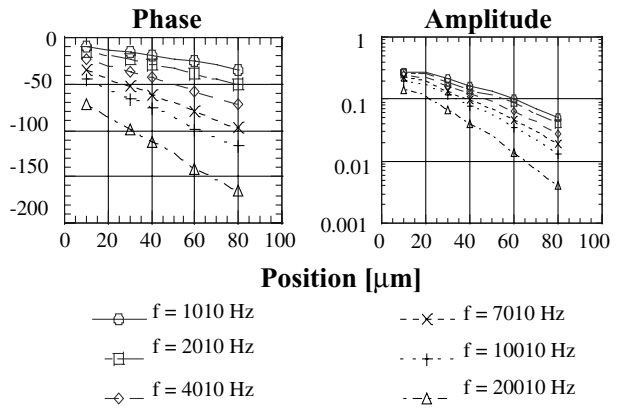


Fig. 5. Phase and amplitude reflectometric measurements with periodic activation of the heat source.

Following the axis of the picture, transient and AC measurements have been performed. Both results are shown in the next figures: Fig. 5 shows the amplitude (due to the passivation layer, the vertical axis is proportional to $T_{AC}$ as the exact value of $\psi$ is not known), and phase ($\phi$) of the sinusoidal temperature as a function of the distance from the heat source for different activating frequencies. In this example, the diameter of the laser beam is 3 μm, therefore measurements can be assumed to be punctual. The linear behaviour of the phase in relation to the distance that is observed when the heat source is activated with a high frequency sinusoidal function has been used in Ref. [24] to locate the heat source with three punctual thermal measurements.

Fig. 6 shows the shape of the thermal disturbance generated by the dissipation of a power pulse of 23 mW during 100 μs. As it can be seen, transient measurements can detect the activation of a heat source.

Scanning an area of the IC, thermal maps can be obtained. For instance, Fig. 7 (right) shows a phase map (60 μm × 60 μm) obtained for AC measurements. Comparing the phase map with the layout of the scanned area (left) the activated heat source is easily located. The time needed to extract the images of Fig. 7 is about 1 h.

## 4. Laser interferometer

The probe is an homodyne, actively stabilised Michelson interferometer [22] devoted to microelectronic applications.

The sensitivity is $10^{-16}$ m and operation covers from practically the DC regime to 150 MHz. The measurement range goes from $10^{-16}$ to $10^{-3}$ m. A schematic view of the probe is presented in Fig. 8. A beam from a He–Ne laser is split into a reference arm and a probe arm ended, respectively, by a piezomirror and the sample under test. The sample is mounted on a computer controlled translation stage while the mirror can be moved by a piezoactuator controlled by the feedback loop of the active stabilisation. The two reflected beams coming out of the interferometer interfere on a photodiode. The detected interferometric signal is sent to the active stabilisation. The principle of the active stabilisation consists of controlling the position of the piezomirror in order to compensate for the slow phase shifts between the two interfering beams. In our application it is possible to record either the interferometric signal induced in the photodiode or the voltage applied by the output of the feedback loop to the piezomirror.

Following the axis marked in Fig. 4, transient and AC measurements have been performed. AC measurements are shown in Fig. 9 as a function of the distance from the heat source for different activation frequencies. As in the previous case, the linear behaviour of the phase as been used in Ref. [24] to locate the heat source with three measurements or in Ref. [25] to locate it with goniometric laser probing. Amplitude measurements show dilatations of the surface due to variations of temperature. Transient measurements can also be done. Fig. 10 shows different thermal expansion signals recorded for five given locations

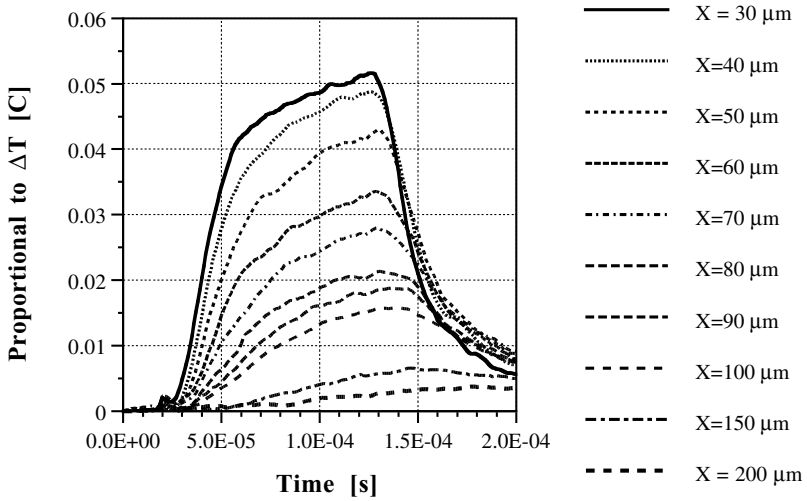


Fig. 6. Transient thermal measurements. Power dissipated by the heat source: 23mW.

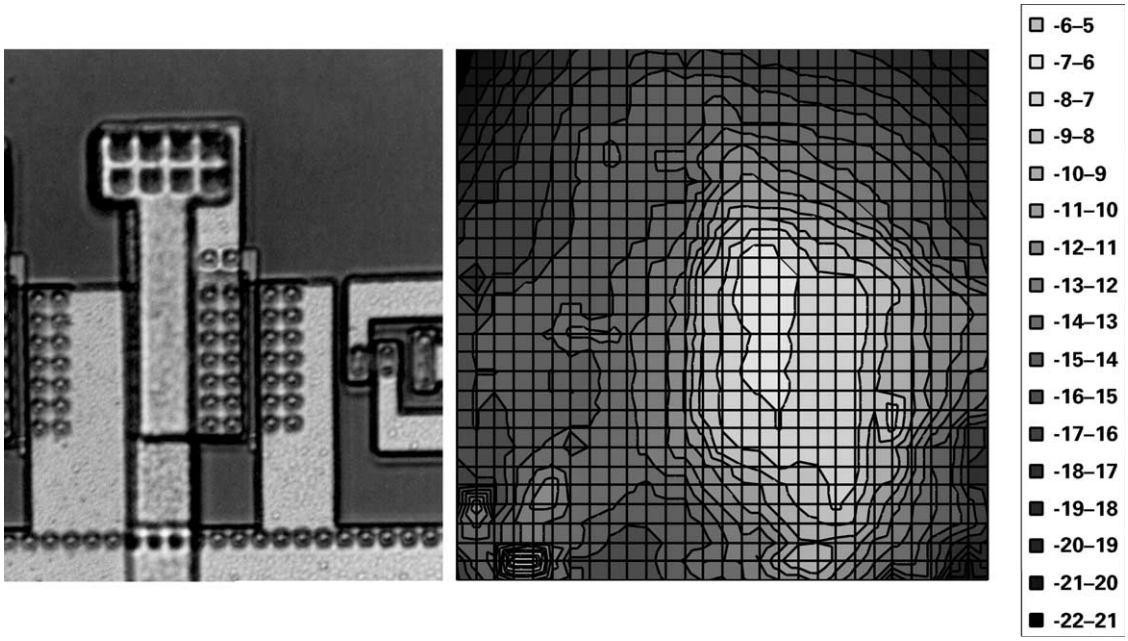


Fig. 7. Phase cartographic map.

in Fig. 3 ($X = 0$, 30, 60, 90 and 120 μm). The diffusion of heat is responsible for the smoothing of the signal as the distance to the source increase.

## 5. Built-in differential temperature sensor

The built-in differential temperature sensor is a variation of a classical BiCMOS operational transconductance amplifier (OTA) and its schematic is shown in Fig. 11. The output voltage of this sensor presents a variation proportional to the difference of temperature between the bipolar transistors Q1 and Q2. Its sensitivity depends on its biasing. For instance, typical simulated analysis provide a sensitivity of $-2.7$ V/°C when through M5 flows a current of 23 μA. Exact value of the sensitivity can be obtained with a calibration procedure.

The bandwidth of the sensor is given by the high impedance node $V_{out}$:

$$f_C = \frac{1}{2\pi R_{out} C_{out}}$$

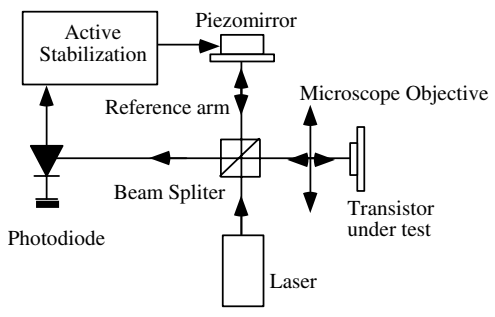


Fig. 8. Interferometric set-up surface displacement.

As any OTA, both the dynamic (bandwidth, slew-rate) and static performances (sensitivity, output resistance) depend on the bias of the circuit. More details about this circuit can be found in Ref. [23].

Fig. 12 shows the layout of the circuit. There, the distance between the bipolar transistors that act as a temperature transducer is 500 μm to ensure that the activation of a heat source generates a difference of temperature at the bipolar transistor's location.

AC, transient and DC measurements have been performed. Fig. 13 shows AC measurements: amplitude and phase of the first harmonic of the $V_{out}$ signal are plotted as a function of the distance between the activated heat source and the bipolar transistor Q1 (looking at Fig. 12, the left side heat sources have been sequentially activated), for five different activation frequencies. As in Sections 3 and 4, the phase exhibits a linear behaviour with the distance.

The bode diagram obtained between the power function dissipated by the heat source and the output voltage of the sensor is plotted in Fig. 14 for two heat sources, placed at 80

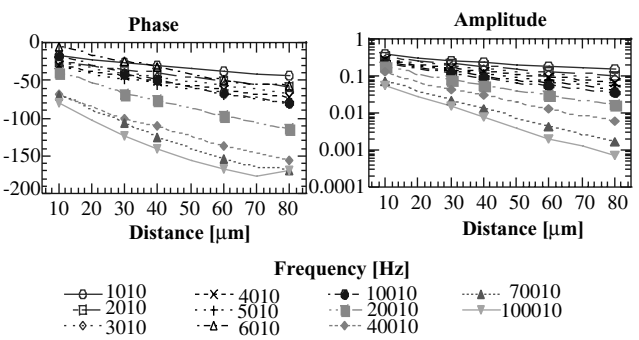


Fig. 9. Phase and amplitude interferometric measurements with periodic activation of the heat source.

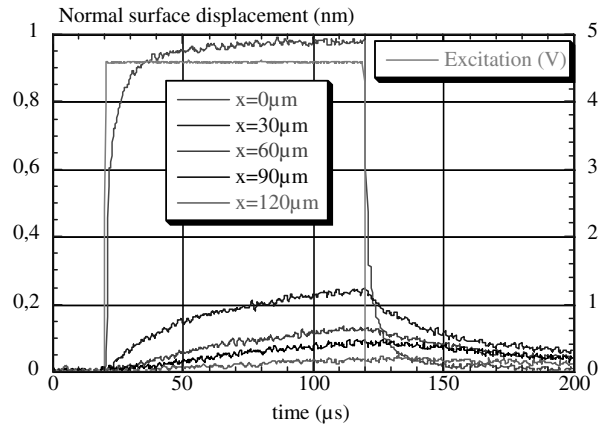


Fig. 10. Transient interferometric measurements.

and 100 μm from the bipolar transistor Q1 (580 and 600 μm from the bipolar transistor Q2) respectively. Note that this graph shows the effect of two transfer functions connected in series: the transfer function of the thermal coupling between the heat source and the bipolar transistors and the transfer function of the sensor itself.

Fig. 15(a) shows DC temperature measurements. The plot shows variation in the sensor's output voltage as a function of the distance between the active heat source and the closest bipolar transistor. In that case, the heat sources were sequentially activated and its power dissipation was 5 mW. The exact location of the heat sources is indicated with dots. Fig. 15(b) shows transient temperature measurements: the dynamic output voltage variation is plotted when a heat source placed at 77 μm from Q1 dissipates 23 mW for four different durations.

## 6. Evaluation

In order to evaluate the efficiency of an IC thermal testing methodology, several parameters have to be taken into account among them: sensitivity, applicability (ability to perform measures at any location of the IC), cost, bandwidth capability, complexity of the equipment required to get the measures, hot spot location ability, required silicon overhead, visual access capability, lateral resolution, measuring time, sample process requirements, effect of superficial layers on the measure, etc.

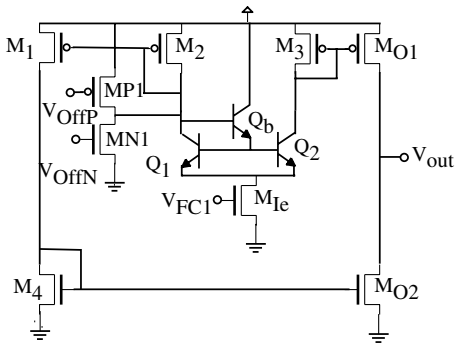


Fig. 11. Schematic of the differential built-in temperature sensor.

In terms of sensitivity, the DBT sensors exhibit the highest sensitivity (0.2 mK) in the sensing point. This technique is based on the placement of a limited number of sensors in the CUT, allowing the calculation of temperature (phase and amplitude) at points around the sensor matrix data through the heat propagation mechanism laws. The LRT and LIT techniques present lower sensitivity in the measuring point but they have the advantage to reach directly to all the points of interest always inside the scanning area. The lowest sensitivity (0.05 K) is exhibited by the SThM technique, compensated in part also by its scanning base.

The three scanning techniques, SThM, LRT and LIT offer a high applicability and location ability because of its capability to generate full thermal surface maps of the accessed area. The topographic abilities of the SThM

Table 1
Comparison of the different technique's performances

| | SThM | LRT | LIT | DBT |
|---|---|---|---|---|
| Bandwidth | 10 kHz | 150 MHz | 150 MHz | 1 MHz |
| Area overhead | No | No | No | Yes |
| Sensitivity | 0.05 K | 1 mK | 1 fm | 0.2 mK |
| On line test | No | No | No | Yes |
| Visual access | Yes | Yes | Yes | No |
| Punctual | Yes | Yes | Yes | Yes |
| Topographic | Yes | No | Yes | No |
| Transient measurements | Yes | Yes | Yes | Yes |
| AC measurements | Yes | Yes | Yes | Yes |
| DC measurements | Yes | No | No | Yes |
| Cost | $$$ | $$ | $$ | $ |
| 2D Maps | Yes | Yes | Yes | No |
| 2D Maps procedure | Continuous scanning | Point by point | Point by point | None |
| Laboratory environment | Yes | Yes | Yes | No |
| Affected by superficial layers | Yes | Yes | Yes | No |
| Dynamic range | up to 500 °C | $\Delta T < 10^2$ K | $\Delta x < 10^{-3}$m | $\Delta T < 2$ K |
| Lateral resolution | 50 nm | 1 μm | 1 μm | No |

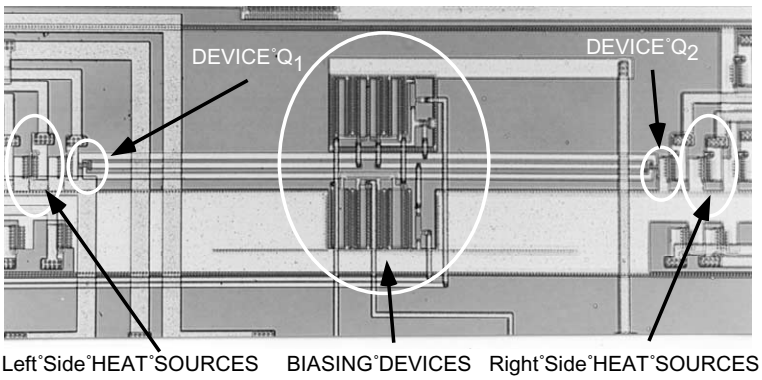


Fig. 12. Layout of the differential temperature sensor.

technique offer easy identification of the heat source, metal lines and adjacent devices. The resolution of the SThM is around 50 and 500 nm for both the LRT and LIT. In terms of applicability the DBT has the lowest level, as the sensors are placed in the design phase of the circuit (following design for thermal testing goals). However, this last approach is not affected by metal, oxide and passivation layers placed over the silicon (the propagation of heat is made mainly through substrate with a good thermal coupling with the semiconductor sensors). In the surface scanning techniques, the measures are somehow or other affected by these layers, either spreading heat and reducing the sensitivity and accuracy of measures or modifying the proportionality constant between the temperature and the sensor's output magnitude. It is interesting to note that for LRT and DBT techniques, phase AC temperature measurements have the advantage in front of amplitude measurements that do not need calibration phase.

The complexity of the required equipment is narrowly related with cost. The three scanning techniques need a laboratory environment and a direct access to the silicon surface (therefore, the package has to be removed) and the three imply costly and complex equipment as well as technician experience. The cost of the SThM equipment is much higher than the correspondent to LRT and LIT. In terms of test procedure cost, the lowest is by far the DBT. This technique requires a silicon overhead and consequently implies a manufacturing cost but the equipment remains cheap (conventional electronic instruments), and is compatible with remote advanced testing access techniques as JTAG mechanisms. The measurement can be applied both in the manufacturing phase and in the in-field maintaining phase with the same requirements and always with the circuit package.

In relation with the capability to follow and measure dynamic thermal signals (bandwidth), the fastest techniques are the LIT and the LRT with possibilities up to 150 MHz. The DBT bandwidth ranges around 1 MHz. Because of Pt sensor thermal inertia, SThM is much slower than the other techniques (10 kHz).

Table 1 presents the above mentioned performance parameters regarding to the four measuring techniques. In the table, the rows represent the category or degree of satisfaction for each characteristic. Depending on the type of parameters and the data accessibility the table has been filled with data or qualitative symbols.

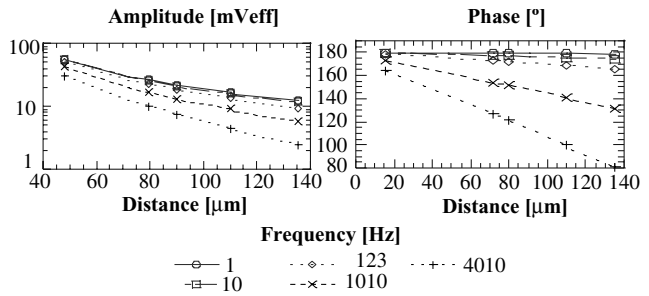


Fig. 13. Phase and amplitude sensor measurements with periodic activation of the heat source.

## 7. Conclusion

Thermal testing has been shown useful in the on-line or

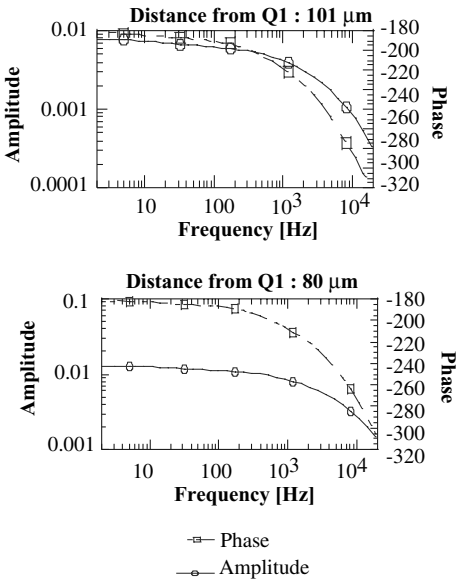


Fig. 14. Bode diagram of the power dissipated by the heat source and the output voltage of the sensor.

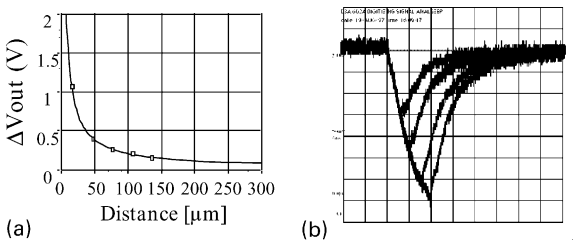


Fig. 15. (a) Static measurements versus distance for a case with 5 mW of power dissipation. (b) Transient measurements when a heat source placed at 77μm from Q1 dissipates 23mW for 30, 50, 80 and 100 μs. (X-axis: 50μs/div; Y-axis: 50mV/div).

off-line test of IC's in presence of intrinsic or extrinsic defects. Four advanced full or partially automated measuring techniques have been exposed, showing their working principles and the measuring performance levels.

The selection of the technique used to measure or diagnose a defective IC has to refer to the set of mentioned characteristics and the application requirements. The four techniques appear as strongly complementary, they also allow high time (150 MHz) and spatial (50 nm) resolutions and a remarkable sensitivity (1 mK) which are not reached by conventional IC temperature testing techniques.

## References

[1] J. Soden, R.E. Anderson, IC failure analysis: techniques and tools for quality and reliability improvement, Proc. IEEE 81 (1993) 703–715.
[2] S. Chandrasekhar, Liquid Crystals, Cambridge University Press, Cambridge, 1992.
[3] V. Székely, S. Ress, A. Poppe, S. Török, D. Magyari, Zs. Benedek, K. Torki, B. Courtois, M. Renz, New approaches in the transient thermal measurements, Microelectron. J. 31 (2000) 727–733.
[4] P.E. Bagnoli, C. Casarosa, M. Ciampi, E. Dallago, Thermal resistance analysis by induced transient (TRAIT) method for power electronic devices thermal characterization. Part I. Fundamentals and theory, IEEE Trans. Power Electron. 13 (6) (1998) 1208–1219.
[5] P.E. Bagnoli, C. Casarosa, M. Ciampi, E. Dallago, Thermal resistance analysis by induced transient (TRAIT) method for power electronic devices thermal characterization. Part II. Practice and experiments, IEEE Trans. Power Electron. 13 (6) (1998) 1220–1228.
[6] V. Székely, M. Rencz, Image processing procedures for the thermal measurements, IEEE Trans. Compon. Packag. Technol. 22 (2) (1999) 259–265.
[7] J. Hiatt, A method of detecting hot spots on semiconductors using liquid crystals, Proc. Int. Rel. Phys. Symp. April (1981) 130–133.
[8] P. Kolodner, J.A. Tyson, Remote thermal imaging with 0.7-mm spatial resolution using temperature-dependent fluorescent thin film, Appl. Phys. Lett. 42 (1) (1983) 117–119.
[9] P. Kolodner, J.A. Tyson, Microscopic fluorescent imaging of surface temperature profiles with 0.01 °C resolution, Appl. Phys. Lett. 40 (9) (1982) 782–784.
[10] J. Lai, M. Chandrachood, A. Majumdar, J.P. Carrejo, Thermal detection of device failure by atomic force microscopy, IEEE Electron Device Lett. 16 (7) (1995) 312–315.
[11] J. Altet, A. Rubio, Built-in dynamic thermal testing technique for ICs, Electron. Lett. 32 (21) (1996) 1982–1984.
[12] D.H. Lee, Thermal analysis of integrated-circuit chips using thermographic imaging techniques, IEEE Trans. Inst. Meas. 43 (6) (1994) 824–829.
[13] J. Kölzer, J. Otto, Electrical characterization of megabit DRAMs. Part 2. Internal testing, IEEE Des. Test Comput. December (1991) 39–51.
[14] M. Nishigushi, et al., Precision comparison of surface temperature measurement techniques for GaAs IC's, IEEE Trans. Comput. Hyb. Man. Tech. 16 (5) (1993) 543–549.
[15] Pentium® III Processor Active Thermal Management Techniques, Order # 273405-001, August 2000, http://www.intel.com.
[16] Intel® Pentium® 4 Processor in the 423-pin Package, Thermal Design Guidelines, Order # 249203-001, November 2000.
[17] V. Székely, Cs. Márta, Zs. Kohári, M. Rencz, CMOS sensors for on-line thermal monitoring of VLSI circuits, IEEE Trans. VLSI Syst. 5 (3) (1997) 270–276.
[18] S. López-Buedo, J. Garrido, E. Boemo, Thermal testing on reconfigurable computers, IEEE Des. Test Comput. January–March (2000) 84–91.
[19] A. Majumdar, Annu. Rev. Mater. Sci. 29 (1999) 505–585.
[20] W. Claeys, S. Dilhaire, V. Quintard, J.P. Dom, Y. Danto, Thermo-reflectance optical test probe for the measurement of current-induced temperature changes in microelectronic components, Quality Reliab. Engng Int. 9 (1993) 303–308.
[21] V. Quintard, G. Deboy, S. Dilhaire, D. Lewis, T. Phan, W. Claeys, Laser beam thermography of circuits in the particular case of passivated semiconductors, Microelectron. Engng 31 (1996) 291–298.
[22] W. Claeys, S. Dilhaire, S. Jorez, L.D. Patiño Lopez, Laser probes for the thermal and thermomechanical characterization of microelectronic devices, Microelectron. J. 32 (10–11) (2001) 891–898.
[23] J. Altet, A. Rubio, S. Dilhaire, E. Schaub, W. Claeys, BiCMOS thermal sensor circuit for built-in test purposes, IEE Electron. Lett. 34 (13) (1984) 1307–1309.
[24] S. Dilhaire, E. Schaub, W. Claeys, J. Altet, A. Rubio, Localisation of heat sources in electronic circuits by microthermal laser probing, Int. J. Therm. Sci. 39 (2000) 544–549.
[25] S. Dilhaire, J. Altet, S. Jorez, E. Schaub, A. Rubio, W. Claeys, Fault localisation in ICs by goniometric laser probing of thermal induced surface waves, Microelectron. Reliab. 29 (1999) 919–923.